Nanoscale

Accepted Manuscript

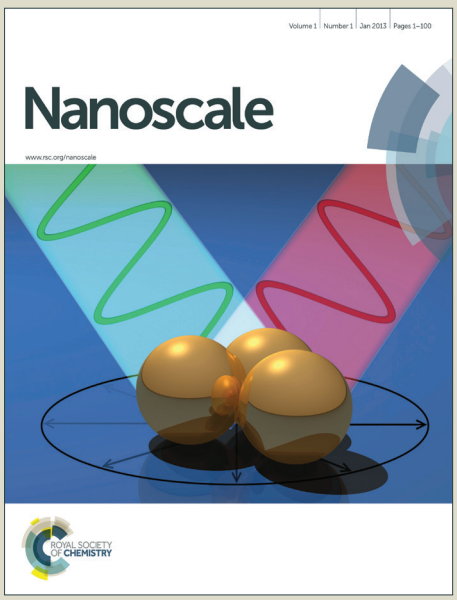

ROYAL SOCIETY OF CHEMISTRY

www.rsc.org/nanoscale

Cite this: DOI: 10.1039/c0xx00000x

www.rsc.org/xxxxxx

ARTICLE TYPE

γ-Fe_2O_3-MWNT/Poly (*p*-PhenyleneBenzobisoxazole) Composites with Excellent Microwave Absorption Performance and Thermal Stability

Yi Chen,[a] Xiaoyun Liu,*[a,b] Xiaoyang Mao,[a] Qixin Zhuang,*[a,] Zhong Xie,[c] and Zhewen Han[a]

Received (in XXX, XXX) XthXXXXXXXXX 20XX, Accepted Xth XXXXXXXXX 20XX

DOI: 10.1039/b000000x

Ferromagnetic γ-Fe_2O_3 nanoparticles were successfully loaded into multi-walled carbon nanotubes (MWNTs) as probed by transmission electron microscopy. Upon incorporation of the γ-Fe_2O_3-MWNTs into poly (*p*-phenylenebenzobisoxazole) (PBO), a conjugated polymer with high mechanical strength, outstanding thermal and oxidative stability, microwave absorbing materials were obtained. Attributing to the special structure of the γ-Fe_2O_3-MWNTs, synergistic effects on dielectric loss and magnetic loss, and a better matched characteristic impedance of the composites were achieved. The optimal minimum reflection loss reached -32.7 dB at 12.09 GHz on a composite containing 12 wt.% γ-Fe_2O_3-MWNTs with thickness of 2.7 mm and the corresponding bandwidth below -5 dB was 6.2 GHz. This demonstrated its potential applications low-density microwave absorbing materials operated under extreme environment.

Introduction

The wide spread use of various electronic equipment and the rapid development of electromagnetic technology attracted overwhelmingly intensive research interests on electromagnetic wave absorbing and shielding materials which may find their potential applications in civil (reduction of electromagnetic interference among components and circuits reduction of the back-radiation of microstrip radiators) and military (reduction of radar signature of aircraft, ships, tanks, and targets) fields.[1] Since the first report of carbon nanotubes (CNTs) in 1991, considerable studies have been published on their use in energy storage devices,[2] catalysts,[3] sensors,[4] optoelectronic[5] and electrorheological fields.[6] In addition, the special structure and size effects contribute to their excellent electrical conductivity and mechanical properties,[7] which facilitates its application in microwave absorbing field. However, since CNTs are nonmagnetic materials, their microwave absorption capability originates either from polarization, ohmic losses, or from multiple scattering due to the large specific surface area. Therefore, synthetic strategies were proposed to prepare CNTs composites with ferromagnetism and good conductivity by either interior filling or exterior coating with magnetic particles. A great variety of magnetic metal and metallic oxide particles have been selected to produce functionalized CNTs microwave absorber. Usually, transition metal elements, such as Fe, Ni and Co, play an important role modification of CNTs with enhanced electromagnetic properties, comparable to those of other metal (Ag and Sn)[8, 9] and rare earth oxide (Sm_2O_3 and Er_2O_3)[10, 11] loaded multi-walled carbon nanotubes (MWNTs). Due to the environmental friendliness, abundant natural supply, high magnetization and a wide range of magnetic anisotropy, γ-Fe_2O_3 is highly desirable for magnetic applications. Although numerous studies on the microwave absorption properties of the γ-Fe_2O_3 and its composites with other nanoparticles (graphite oxide, $BaTiO_3$, etc.) were reported in different matrix (polyaniline, phenolic resin, carbon matrix and PVC)[12-15], seldom have the magnetic properties and microwave absorbability of the γ-Fe_2O_3 loaded CNTs absorber been reported. On the other hand, as a kind of conjugated polymers with excellent thermal stability, environmental stability and mechanical properties, poly (*p*-phenylenebenzobisoxazole) (PBO) has wide spread potential applications in many fields. The composites of magnetic materials within a PBO matrix are expected to have potential applications due to their excellent microwave absorption performance and thermal stability.

In this communication, MWNTs were loaded with magnetic nanoparticles (γ-Fe_2O_3) via wet chemical method. Then, γ-Fe_2O_3-MWNTs/PBO composites were fabricated by premixing γ-Fe_2O_3-MWNTs and poly (o-hydroxyamide) (PHA, the precursor of PBO) in solution followed by in-situ cyclodehydration in the bulk at elevated temperature. The uniform dispersion of magnetic γ-Fe_2O_3 nanoparticle in PBO matrix is achieved by physical isolation effect of the MWNTs, different from the simple mixing of each component. Many studies focused on electromagnetic wave absorbing and shielding materials prepared by γ-Fe_2O_3 and its composites, and only few researchers regarded the γ-Fe_2O_3 loaded MWNTs as the filler and studied the electromagnetic properties of its composites. To the best of our knowledge, the optimal minimum reflection loss (RL) of the pure γ-Fe_2O_3 with a specific dendritic microstructure is -50.0 dB at around 9.2 GHz with sample thickness of 4 mm. In our study, however, when the concentration of the functionalized MWNTs is 12 wt.%, the microwave absorption of the composites reached -32.7 dB (RL_{min}) at 12 GHz with thickness of only 2.7 mm, better than that of the γ-Fe_2O_3 modified microwave absorbing materials reported previously (RL_{min} = -32.0 dB for γ-Fe_2O_3/carbon nanocomposites,[12] where more carbon materials and/or nanoparticles were required in the absence of polymer matrix,

while in our study, the total content ration of MWNTs and γ-Fe_2O_3 in PBO based composite is below 15 wt.%). Furthermore, it is much better than that of Fe/Fe_3C-MWNTs composites (RL_{min} = -14 dB) or Fe filled MWNTs (RL_{min} = -22.73 dB),[16] although it was believed that the reflection loss of Fe/Fe_3C-MWNTs is much better than that of γ-Fe_2O_3-MWNTs after a reduction.[17] Furthermore, this data is also superior compared to many other reported microwave absorption properties of unfunctionalized representative carbon nanomaterials.[16, 18-21] Up to now, this is the most effective strategy to prepare a material with excellent microwave absorption property with such little concentration of loaded MWNTs compared to other γ-Fe_2O_3 decorating methods. All these can be ascribed to the special morphology and structure of the loaded MWNTs, the effective complementarity between dielectric loss and magnetic loss, and the optimal matched characteristic impedance of the composites.

Experiment

Materials

MWNTs (20-40 nm, 97% pure) prepared by chemical vapor deposition (CVD) were purchased from Shenzhen Nanoport Company. Terephthaloyl Chloride (TPC) was provided by Sigma-Aldrich Chemical Co.. N,N-dimethylformamide (DMF) was purified by vacuum distillation from calcium hydride and stored in a desiccator prior to use. Other reagents and solvents were used as received.

Purification and Functionalization of MWNTs

The MWNTs were refluxed in concentrated nitric acid for 24 h to remove the impurities such as amorphous carbon and catalyst particles generated during manufacturing MWNT. Thus, MWNTs were coated with many functional groups such as hydroxyl (-OH) and carboxyl (-COOH), and terminals of MWNTs channel were broken open. Then, the solution was centrifuged and washed copiously with deionized water until the washout was neutral. The precipitates were dried under vacuum at 100 °C for 24 h. And the purified MWNTs with open terminals were thus obtained.

Next, the purified MWNTs (200 mg) and $Fe(NO_3)_3$ (1.6 g) was uniformly dispersed in concentrated nitric acid (10 mL) and the suspension was refluxed for 5 h, followed by centrifugation and drying under vacuum at 100 °C for 24 h. After thorough grinding, the solid was heated from room temperature up to 400 °C at rate of 1 °C/min and baked at 400 °C for 5 h in a tube furnace under argon atmosphere, followed by cooling arbitrarily down to ambient temperature. The obtained solid was dispersed in deionized water by ultrasonication, and collected with Buchner funnel followed by copious wash with water. The collected solid was dried at 100°C for 12 h under vacuum, yielding black powder (γ-Fe_2O_3-MWNTs).

Synthesis of PHA

PHA, the precursor of PBO, was prepared with an aromatic dicarboxylic active diester and bis(*o*-aminophenol)via a typical synthetic scheme (Scheme S1†). 4, 6-Diaminoresorcinol dihydrochloride (DAR·2HCl) (1.065 g, 5 mmol) was dissolved in anhydrous DMF (20 mL) in a flask (100 mL) equipped with an ice bath at 0-5 °C under magnetic stirring. Solution containing terephthaloyl chloride (TPC) (1.015 g, 5 mmol) and pyridine (2 mL) was added to the flask dropwise. The reaction was carried out at -10-0 °C for the first 2 h and at room temperature overnight under nitrogen. The reaction mixture gradually became viscous as polycondensation proceeded. The resulting viscous polymer solution was poured slowly into excess amount of deionized water under vigorous stirring. The fibrous precipitate was collected with Teflon filter and washed repeatedly with deionized water, followed drying under vacuum overnight.

Preparation of γ-Fe_2O_3-MWNTs/PBO composites

First, PHA and γ-Fe_2O_3-MWNTs were dispersed uniformly in DMF at a designated ratio. The solution was then poured into excess deionized water with stirring, and the γ-Fe_2O_3-MWNTs/PHA precipitate was collected by filtration and washed repeatedly with water, and dried under vacuum at 60 °C. The complete conversion to γ-Fe_2O_3-MWNTs/PBO was achieved by heating the γ-Fe_2O_3-MWNTs/PHA at 300 °C for 5 h under nitrogen, yielding brown solid. For comparison, MWNTs/PBO composite without γ-Fe_2O_3 was also fabricated under nitrogen through the same procedures.

Sample preparation for microwave absorption performance analysis

A sample containing 30 wt.% of prepared composites was pressed into a ring with outer diameter of 7 mm, inner diameter of 3 mm, and thickness of 2 mm for microwave absorption measurement, in which paraffin wax was used as binder.

Instrumentation

Fourier transform infrared (FT-IR) spectra were recorded on KBr pellet support with a Nicolet 5700 Fourier transform spectrophotometer. Nuclear magnetic resonance (NMR) spectra were recorded on a Bruker Avance III operating at 400 MHz for ^{1}H-NMR, using dimethyl sulfoxide (DMSO)-d_6 as solvent. The morphology was probed by Transmission Electron Microscope (TEM) (JEM-2100F). The X-ray diffraction (XRD) pattern was collected on a D/MAX-2550 VB/PC X-ray diffractometer with Cu/K-α1 radiation. Thermogravimetric analysis (TGA) was conducted using a DuPont model 951 thermogravimetricanalyzer. Gel permeation chromatography (GPC) was performed on a Waters 515 GPC (mobile phase, DMF) equipped with a UV detector using polystyrene standards. The magnetic properties were investigated with a vibrating sample magnetometer (VSM) (Lake Shore 7407) at room temperature. For microwave absorption measurements, an 8722ES vector network analyser was applied to determine the complex relative permeability $\mu_r = \mu'\text{-}j\mu''$ and the complex relative permittivity $\varepsilon_r = \varepsilon'\text{-}j\varepsilon''$ in the frequency range of 2-18 GHz for calculation of reflection loss and impedance.

Results and discussions

Morphology of γ-Fe_2O_3-MWNTs

In concentrated nitric acid, ferric nitrate solution was introduced into the cavity of the MWNTs through capillary action. After heat treatment, ultrasonication and washing with water, most nanoparticles on the surface of the MWNTs were removed, while those in the inner capillary of MWNTs were immobilized by the

restriction effect. Compared to those reported previously,[17, 22] a TEM image with better contrast between γ-Fe_2O_3 and MWNTs was obtained as shown in Fig. 1a. To make it clear, a schematic view in which γ-Fe_2O_3 nanoparticles were encapsulated by tri-layered CNTs was proposed in Fig. 1b. A HRTEM image (Fig. S1†) of loaded MWNTs showed that nanoparticles were orientated randomly along the MWNTs capillary, and uniformly separating the long and narrow cavity into polyporous structure, due to the overflowed gas generated from the decomposition of iron salt. Individual crystals tended to be either spherical or ellipsoidal in shape with diameters ranging from 5 to 15 nm, approximating to the inner diameters of the cross-sections of MWNTs (Fig. 1c). Inevitably, several nanoparticles can be observed on the surface of the MWNTs. By measuring the spacing of lattice fringes of individual crystallites relative to the *d*-spacing of the carbon nanotube wall before and after functionalization (corresponding to 0.34 nm in Fig. S1 and S2†), other lattice fringes can be indexed (dark spots in Fig. S1†) to specific lattice planes anticipated for γ-Fe_2O_3. This polyporous structure is the source of multiple scattering and induces interfacial polarization, and the local properties of nanoparticles are greatly enhanced by the quantum confinement effect. Meanwhile, the discrete energy levels of the encapsulated nanoparticles could absorb the microwave energy through electrons hopping.[1] Thus, this well-defined special structure laid a solid foundation for the improvement in the microwave absorption performance of the MWNTs. In the XRD pattern of γ-Fe_2O_3-MWNTs (Fig. 2b), the diffraction peaks at 2θ=30.22°, 35.60°, 43.34°, 53.66°, 57.28° and 62.92°, can be well indexed to (220), (311), (400), (422), (511) and (440) crystal faces of γ-Fe_2O_3, respectively, matching the maghemite γ-Fe_2O_3 (JCPDS card 39-1346)[23]. Peaks at 26.18°and 43°can be indexed to the characteristic crystal faces ((002) and (101)) of MWNTs.

Structure characterization of PHA

PHA, precursor of the PBO, was prepared according to a previously reported method.[24, 25] Chemical structures of both PHA and PBO were confirmed by FT-IR (Fig. 3). As shown in the spectra, the broad absorption band between 3400 and 3000 cm^{-1} was assigned to the -OH stretching and -NH_2 stretching vibrational motion. The absorption bands at 1689 and 1285 cm^{-1} were assigned to the -C=O and -C-N stretching vibrational motion in amide groups, indicating that PHA was successfully prepared. The characteristic absorption bands of benzene ring were observed at 1575, 1510 and 1426 cm^{-1}. As for PBO, the absorption bands at 1629, 1364 and 1267 cm^{-1} assigned to the -C=N, C_{Ar}-N and C-O stretching vibrational motion were also observed, corresponding to the characteristic absorption of oxazole ring. Therefore, complete conversion of PBO from PHA via a thermalcyclodehydration can be confirmed. For PBO, the absorption bands of benzene ring shifted to 1561, 1510 and 1426 cm^{-1}, respectively. Furthermore, the chemical structure of PHA was also characterized by ^{1}H-NMRas shown in Fig. S3†, in which all the protons on the polymer backbones could be well assigned to the expected chemical structure. The characteristic signals of amide and hydroxyl groups at 9.60, 9.67 and 10.22 ppm were observed, respectively. In addition, the molecular weights of PHA were $1.122x10^5$ (M_w) and $1.615x10^5$ (M_n) according to GPC result.

Magnetocrystalline anisotropy

To assess the efficiency of γ-Fe_2O_3 in improving the magnetic properties of MWNTs and corresponding composites, the field-dependent magnetization (*M-H*) curves were obtained at room temperature (Fig. 4). Saturation magnetization (*Ms*, 0.8355 emu/g) and coercivity (*Hc*, 27.94 Oe) of MWNTs were greatly improved in the presence of γ-Fe_2O_3 (*Ms* and *Hc* of γ-Fe_2O_3-MWNTs being 6.829 emu/g and 163.06 Oe, respectively). According to Stoner - Wohlfarth theory,[26] the magnetocrystalline anisotropy constant *K* was given as follows:

$$K = \frac{\mu_O M_S H_C}{2} \quad (1)$$

where μ_o is the universal constant of permeability in free space, $4\pi\times 10^{-7}$ Hm^{-1}.The anisotropy field of MWNTs was increased by a factor of 47.4 after functionalization with γ-Fe_2O_3 and this value is far greater than those reported previously (γ-Fe_2O_3loaded MWNTs composites with *Ms*= 32.83 $emug^{-1}$ and *Hc* = 12.5 Oe) .[17] *Hc* is a key parameter in assessing the magnetic properties of a material, and materials with high *Hc* values are considered to possess a high-frequency resonance.[27] For γ-Fe_2O_3-MWNTs/PBO, the *Ms* (0.4850 emu/g) is significantly higher than that of MWNTs/PBO (0.03082 emu/g) as shown in Fig. 4b, and it is a unique character of ferromagnetic materials. Inevitably, benefiting from the intrinsic character of γ-Fe_2O_3-MWNTs, *Hc* and residual magnetization (*Mr*) of γ-Fe_2O_3-MWNTs/PBO (271.43 Oe, 0.1803 emu/g) are much higher than that of MWNTs/PBO (120.59 Oe, 0.007272 emu/g). Therefore, γ-Fe_2O_3-MWNTs/PBO should possess better microwave absorbability.

Microwave absorption performance

The microwave absorption mechanism of the absorbing materials can be attributed to dielectric loss and magnetic loss. In order to reveal the origin of microwave absorption mechanism, real and imaginary parts of permittivity (*ε'* and *ε"*) and permeability (*μ'* and *μ"*) of the composites were measured. Generally speaking, MWNTs have high conductivity and tend to form conducting net works in the composite based on its special morphology. Thus, both *ε'* and *ε"* have a tendency to increase with increasing concentration of γ-Fe_2O_3-MWNTs in the composites (Fig. 5a, 5b). The *ε"* of the three samples reached peak values in varied frequency ranges: 5 wt.% (14.60 – 18GHz), 10 wt.% (10.48 – 18GHz) and 12 wt.% (10.66 – 18GHz), indicating a resonance behaviour which may lead to intense response in the microwave absorption performance. But for the sample containing 15 wt.% γ-Fe_2O_3-MWNTs, *ε'* and *ε"* were significantly high and reached the same order of magnitude as those of pure γ-Fe_2O_3-MWNTs (Fig. S4†), which could be explained by interfacial polarization[28] or Maxwell-Wagner-Sillars (MWS) theories,[29] resulting from the incorporation of highly conductive MWNTs components into the high dielectric constant composites and can account for the inferior microwave absorption performance. Plausibly due to the low concentration of magnetic γ-Fe_2O_3 components in the composites, the real part (*μ'*) and imaginary part (*μ"*) of complex permeability were about 1.0 and 0.0 (Fig. 5c, 5d), respectively. However, when the concentration of γ-Fe_2O_3-MWNTs reached 15 wt.%, a rapid decrease in *μ"* was observed. Similar to the case

of permittivity, the drastic change in μ' and μ'' made no contribution to the impedance matching and would deteriorate the microwave absorption performance. Also, P. Xu et. al.[17] observed that the large increase in ε'' and sharp decrease in μ'' may not lead to better matched characteristic impedance of free space and thus have negative effect on the microwave absorption.

The reflection loss value of these composites can be obtained on the basis of the aforementioned permittivity and permeability according to the transmission line theory, and the absorption performance was calculated as follows:

$$R(dB) = 20\log_{10}\left|\frac{Z_{in}-1}{Z_{in}+1}\right| \quad (2)$$

$$Z_{in} = \left(\frac{\mu_r}{\varepsilon_r}\right)^{1/2} \tanh\left[j\frac{(2\pi fd)}{c}(\mu_r\varepsilon_r)^{1/2}\right] \quad (3)$$

where Z_{in} is the normalized input impedance in free space and at interface, $\varepsilon_r=\varepsilon'-\varepsilon''$ and $\mu_r=\mu'-\mu''$ are the complex permittivity and permeability, c is the velocity of electromagnetic waves in free space, f is the microwave frequency, and $d$is the thickness of the absorbing layer.

Fig. 6 showed the calculated RL curves of composites with different concentrations of γ-Fe_2O_3-MWNTs and varied thicknesses according to equation (2) and (3) based on the aforementioned four parameters, respectively. The insets in Fig.6 (a-f) are the graphs of the dependence of the RL_{min} and the corresponding frequency on the sample thickness, and all the samples followed same manner that the RL_{min} decreased with increasing thickness followed by a reverse trend, except for the sample at concentration of 15 wt.% (Fig.6f). The variation tendency suggests this system could achieve the optimal impedance compatibility at critical point when the thickness is around 2.7 mm, and the poor microwave absorption of the sample at concentration of 15 wt.% resulted from the poor impedance matching, and the abnormal permittivity and permeability mentioned above. Additionally, as shown on the reflection loss curves of the composites, PBO (Fig.S5†) and γ-Fe_2O_3-MWNTs (Fig. S6†), when the concentration of γ-Fe_2O_3-MWNTs was below 10 wt.% or above 12 wt.%, the optimal impedance was incompatible, and the microwave absorption performance of the composites was controlled by the PBO matrix and the functionalized MWNTs, respectively. Fig.7a showed the comparison of microwave reflection loss of all the samples with thickness of 2.7 mm. Due to the aforementioned reasons, two samples (10 wt.% and 12 wt.%) gave positive response in reflection loss and had wide absorption bands in middle or high frequency range. Although the RL_{min} of the 5 wt.% sample reached -33.27 dB at 17.28 GHz, the bandwidth for the RL value below -5 dB was fairly low (2.24 GHz), while the 10 wt.% sample had broad bandwidth (7.47 GHz for RL < -5 dB). And among all the composites, the 12 wt.% sample had the optimal microwave absorption performance, whose RL_{min} reached -32.70 dB at 12.09 GHz and corresponding bandwidth below -5 dB was 6.18 GHz (RL < -10 dB, 11.31- 13.79 GHz). According to the Kubo theory, the energy levels in the load CNTs are not continuous but splitting due to the quantum confinement effect. When an energy level is in the range of microwave energy, the electron absorbs a photon and hop from a low energy level to a higher one.[30] There are many interfaces between the PBO matrix and MWNTs outer surface. The large contact interface was created between the γ-Fe_2O_3 nanoparticles and MWNT capillary in the γ-Fe_2O_3 loaded MWNTs. Therefore, interfacial multipoles contribute to the absorption of the PBO composites containingγ-Fe_2O_3 loaded CNTs. This optimal RL_{min} has surpassed those of many previously reported microwave absorbing carbon nanomaterials (-18 dB for $CoFe_2O_4$/CNTs[18]; -20 dB for Ni/carbon nanocoils[19]; -22.73 dB for Fe/CNT[16]; -25 dB for Fe/CNTs[20] and -27.9 dB for Fe_3O_4/C nanorods[21]). Moreover, the PBO matrix and the low concentration of fillers resulted in low-density composite, advantageous over other microwave absorbers.

Thermogravimetric analysis (TGA)

The as-prepared composites with varied filler concentrations exhibited excellent thermal properties as assessed by TGA (Fig. 7b). Improved thermal stability was observed when the concentration of filler increased and the thermogravimetric turn point was over 400 °C except for the sample containing only 5 wt.% γ-Fe_2O_3-MWNTs (350 °C). The residues of these samples were all over 60% at 800 °C. Especially, when the concentration of γ-Fe_2O_3-MWNTs reached 15 wt.%, the thermal stability of the composite was superior to PBO in the absence of fillers. This thermally stable microwave absorbing material may have potential applications under extreme environment such as radar-invisible missile and outer-space craft.

Conclusions

In conclusion, γ-Fe_2O_3-MWNTs/PBO composites were fabricated by loading carbon nanotubes with magnetic γ-Fe_2O_3 particles and premixing γ-Fe_2O_3-MWNTs and PHA in solution followed by in-situ cyclodehydration in the bulk at elevated temperature. Due to the special morphology and structure of the filled MWNTs, effective complementary balance was achieved between dielectric loss and magnetic loss, and the optimal matched characteristic impedance, RL_{min} reached -32.70 dB at 12.90 GHz with the sample containing 12 wt.% γ-Fe_2O_3-MWNTs. Materials with excellent microwave absorption performance were successfully obtained in the presence of only low dose of γ-Fe_2O_3 loaded MWNTs. Extensive application prospects can be expected in the field of high-frequency microwave absorbing materials demanding low density and improved thermal stability.

Acknowledgement

This work was financially supported by the NSFC (50973028), the SNSF (12ZR1407900), the Innovation Program of Shanghai Municipal Education Commission (12ZZ049), the Basic Innovation Research Program of Science and Technology Commission of Shanghai (13JC1402002) and China Scholarship Council.

Notes and references

(a), Key Laboratory for Ultrafine Materials of Ministry of Education, School of Materials Science and Engineering, East China University of Science and Technology, Shanghai 200237, China. Tel: 86-21-64252464;

E-mail:liuxiaoyun@ecust.edu.cn, qxzhuang@ecust.edu.cn. (b), Roy & Diana Vagelos Laboratories, Department of Chemistry, University of Pennsylvania, Philadelphia, Pennsylvania 19104, USA. (c), Key Laboratory of Superlight Material and Surface Technology, Ministry of Education, Harbin Engineering University, 145, Nantong St., Harbin, 150001, China.

†Electronic Supplementary Information (ESI) available: Experimental details, Scheme S1 and Fig. S1~S6. See DOI: 10.1039/b000000x/

1. F. Qin and C. Brosseau, *J. Appl. Phys.*, 2012, **111**, 061301.
2. C. Wu, X. Huang, X. Wu, L. Xie, K. Yang and P. Jiang, *Nanoscale*, 2013, **5**.
3. A. W. Orbaek, A. C. Owens, C. C. Crouse, C. L. Pint, R. H. Hauge and A. R. Barron, *Nanoscale*, 2013, **5**.
4. S. Park, M. Vosguerichian and Z. Bao, *Nanoscale*, 2013, **5**.
5. Y. Su, J. Du, S. Pei, C. Liu and H. Cheng, *Nanoscale*, 2011, **3**.
6. K. Zhang, Y. D. Liu and H. J. Choi, *Chem. Commun.*, 2012, **48**, 136.
7. G. Sun, L. Zheng, J. An, Y. Pan, J. Zhou, Z. Zhan, J. H. L. Pang, C. K. Chua, K. F. Leong and L. Li, *Nanoscale*, 2013, **5**.
8. D. Zhao, X. Li and Z. Shen, *Mater. Sci. Eng., B*, 2008, **150**, 105.
9. H. Zhu, L. Zhang, L. Zhang, Y. Song, Y. Huang and Y. Zhang, *Mater. Lett.*, 2010, **64**, 227.
10. L. Zhang, H. Zhu, Y. Song, Y. Zhang and Y. Huang, *Mater. Sci. Eng., B*, 2008, **153**, 78.
11. L. Zhang and H. Zhu, *Mater. Lett.*, 2009, **63**, 272.
12. J. Zhou, J. He, T. Wang, G. Li, Y. Guo, J. Zhao and Y. Ma, *J. Alloy. Compd.*, 2011, **509**, 8211.
13. A. P. Singh, P. Garg, F. Alam, K. Singh, R. B. Mathur, R. P. Tandon, A. Chandra and S. K. Dhawan, *Carbon*, 2012, **50**, 3868.
14. Y. E. Moon, J. Yun and H. Kim, *J. Ind. Eng. Chem.*, 2013, **19**, 493.
15. O. Chiscan, I. Dumitru, V. Tura, H. Chiriac and A. Stancu, *IEEE. T. Magn.*, 2011, **47**, 4511.
16. H. Lin, H. Zhu, H. Guo and L. Yu, *Mater. Lett.*, 2007, **61**, 3547.
17. P. Xu, X. J. Han, X. R. Liu, B. Zhang, C. Wang and X. H. Wang, *Mater. Chem. Phys.*, 2009, **114**, 556.
18. R. C. Che, C. Y. Zhi, C. Y. Liang and X. G. Zhou, *Appl. Phys. Lett.*, 2006, **88**, 033105.
19. N. Tang, Y. Yang, K. Lin, W. Zhong, C. Au and Y. Du, *J. Phys. Chem. C*, 2008, **112**, 10061.
20. R. C. Che, L. M. Peng, X. F. Duan, Q. Chen and X. L. Liang, *Adv. Mater.*, 2004, **16**, 401.
21. Y. Chen, G. Xiao, T. Wang, Q. Ouyang, L. Qi, Y. Ma, P. Gao, C. Zhu, M. Cao and H.-B. Jin, *J. Phys. Chem. C*, 2011, **115**, 13603.
22. X. Qi, W. Zhong, C. Deng, C. Au and Y. Du, *Mater. Lett.*, 2013, **107**, 374.
23. G. Sun, B. Dong, M. Cao, B. Wei and C. Hu, *Chem. Mater.*, 2011, **23**, 1587.
24. Y. Chen, Q. X. Zhuang, X. Y. Liu, J. Liu, S. L. Lin and Z. W. Han, *Nanotechnology*, 2013, **24**.
25. Q. Zhuang, X. Mao, Z. Xie, X. Liu, Q. Wang, Y. Chen and Z. Han, *J. Polym. Sci., Part A: Polym. Chem.*, 2012, **50**, 4732.
26. O. Song and Z. J. Zhang, *J. Am. Chem. Soc.*, 2004, **126**, 6164.
27. S. Ohkoshi, S. Kuroki, S. Sakurai, K. Matsumoto, K. Sato and S. Sasaki, *Angew. Chem. Int. Ed.*, 2007, **46**, 8392.
28. P. Murugaraj, D. Mainwaring and N. MoraHuertas, *J. Appl. Phys.*, 2005, **98**, 054304.
29. R. Tamura, E. Lim, T. Manaka and M. Iwamoto, *J. Appl. Phys.*, 2006, **100**, 114515.
30. D. Zhao, J. Zhang, X. Li and Z. Shen, *J. Alloy. Compd.*, 2010, **505**.

Figures captions

Fig.1 TEM images of loaded MWNTs (a) and its schematic view (b), TEM image of purified MWNTs (c)

Fig. 2 XRD patterns of MWNTs (a) and γ-Fe_2O_3-MWNTs (b)

Fig. 3 FT-IR spectra of PHA and PBO

Fig. 4 Field-dependent magnetization (*M-H*) curves of a, MWNTs and γ-Fe_2O_3-MWNTs; b, MWNTs/PBO and γ-Fe_2O_3-MWNTs/PBO at room temperature.

Fig. 5 Real and imaginary parts of permittivity (ε' (a) and ε'' (b)) and permeability (μ' (c) and μ'' (d)) of the composites

Fig. 6 Calculated RL curves of composites with different concentration of fillers (a, 3 wt.%； b, 5 wt.%; c, 8wt.%; d, 10wt.%; e, 12wt.% and f, 15wt.%, respectively) and varied thickness according to a transmission line theory

Fig. 7 (a) Microwave reflection loss of all the samples with thickness of 2.7 mm. (b) TGA curves of the samples under nitrogen

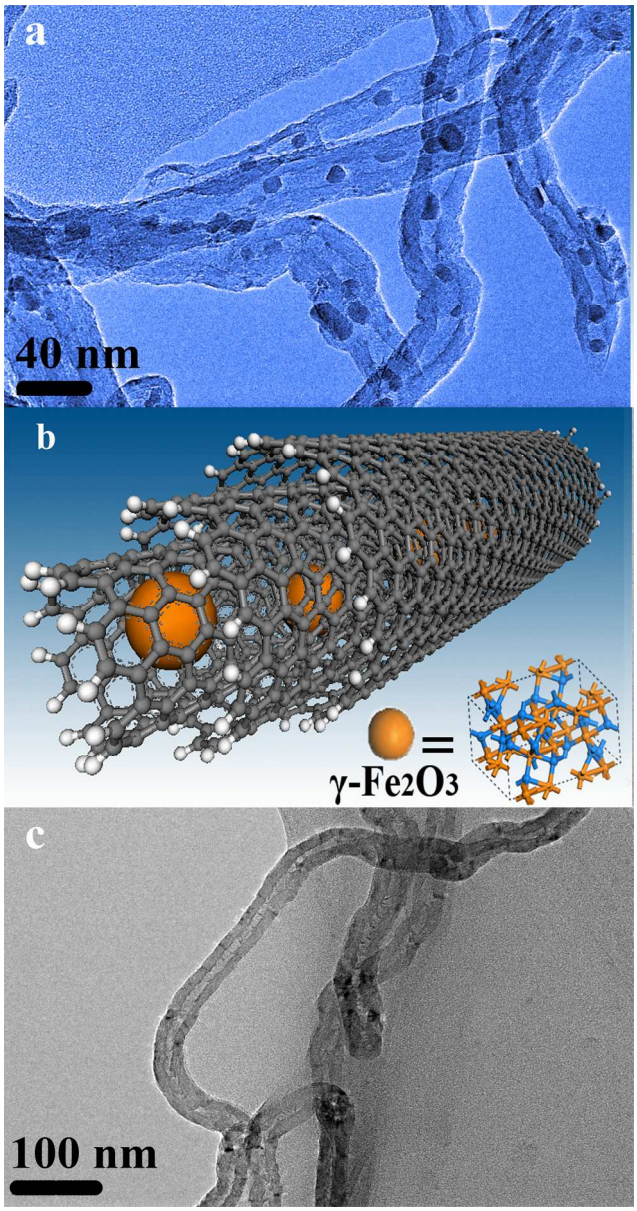

Fig.1 TEM images of filled MWNTs (a) and its schematic view (b), TEM image of purified MWNTs (c)
169x322mm (300 x 300 DPI)

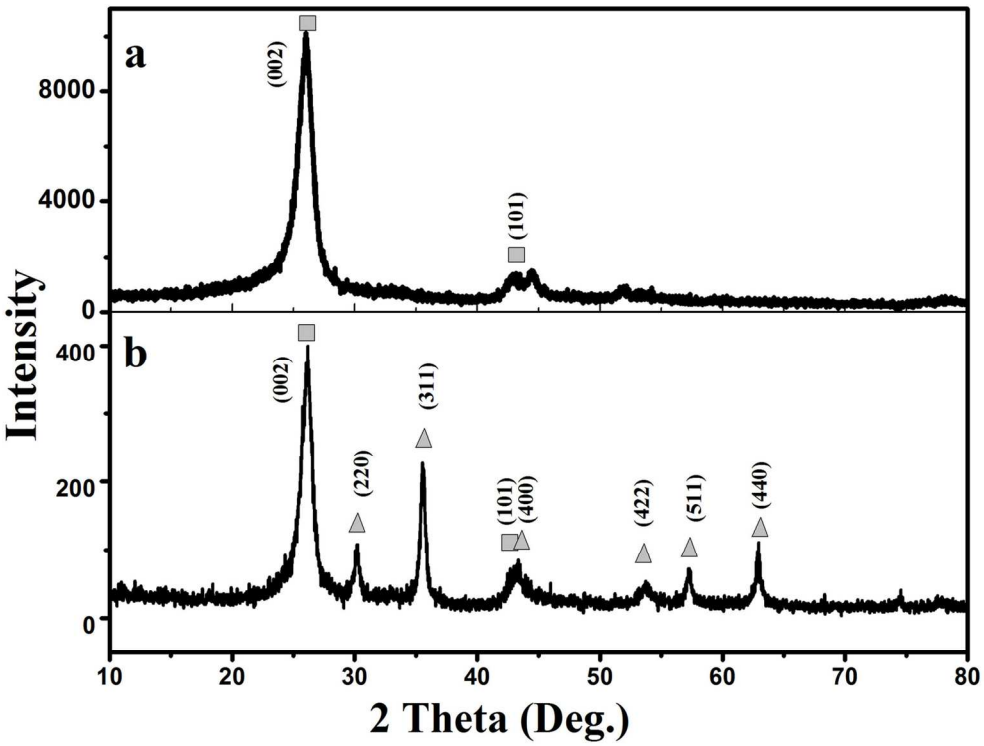

Fig. 2XRD patterns of MWNTs (a) and γ-Fe2O3-MWNTs (b)
68x52mm (600 x 600 DPI)

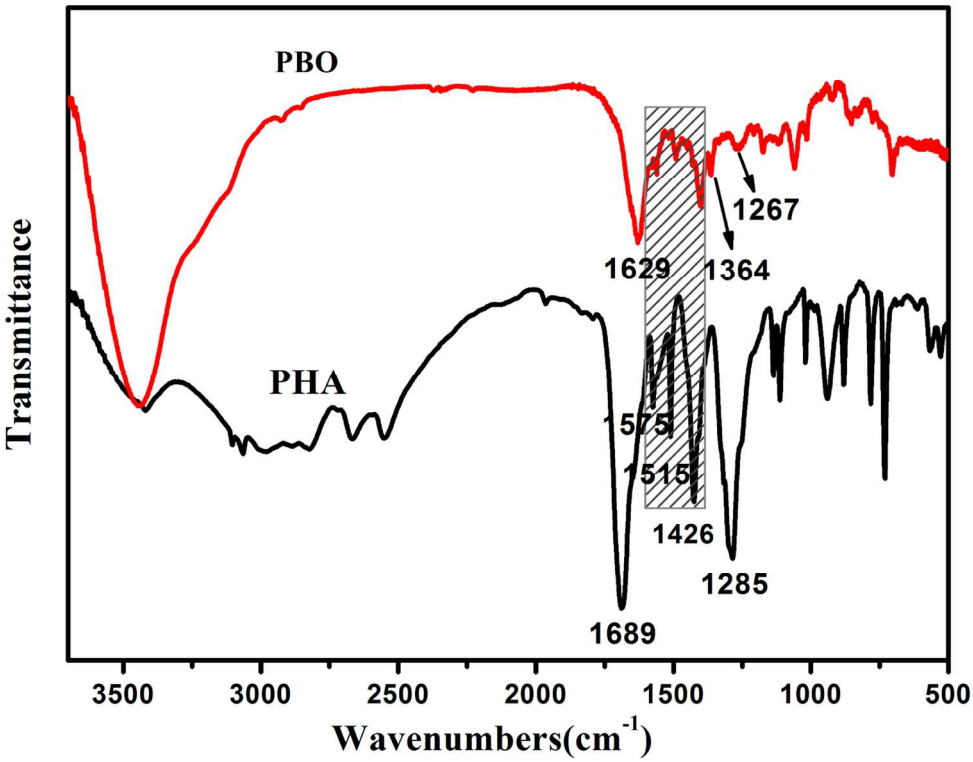

Fig. 3 FT-IR spectra of PHA and PBO
70x55mm (600 x 600 DPI)

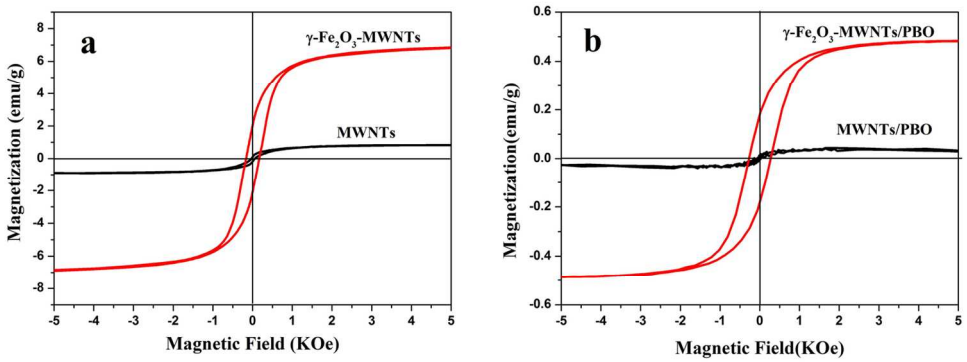

Fig. 4 Field-dependent magnetization (M-H) curves of the samples (a, MWNTs andγ-Fe2O3-MWNTs; b, MWNTs/PBO and γ-Fe2O3-MWNTs/PBO) at room temperature.
68x26mm (600 x 600 DPI)

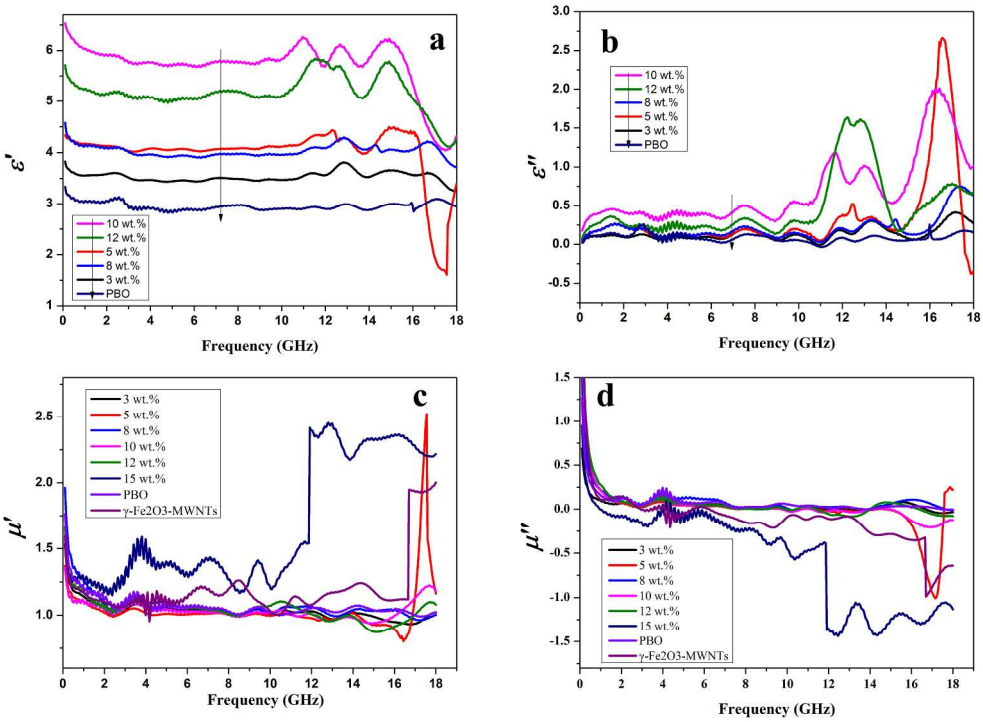

Fig. 5 Real and imaginary parts of permittivity (ε′ (a) and ε″ (b)) and permeability (μ′(c) and μ″ (d)) of the composites
131x97mm (600 x 600 DPI)

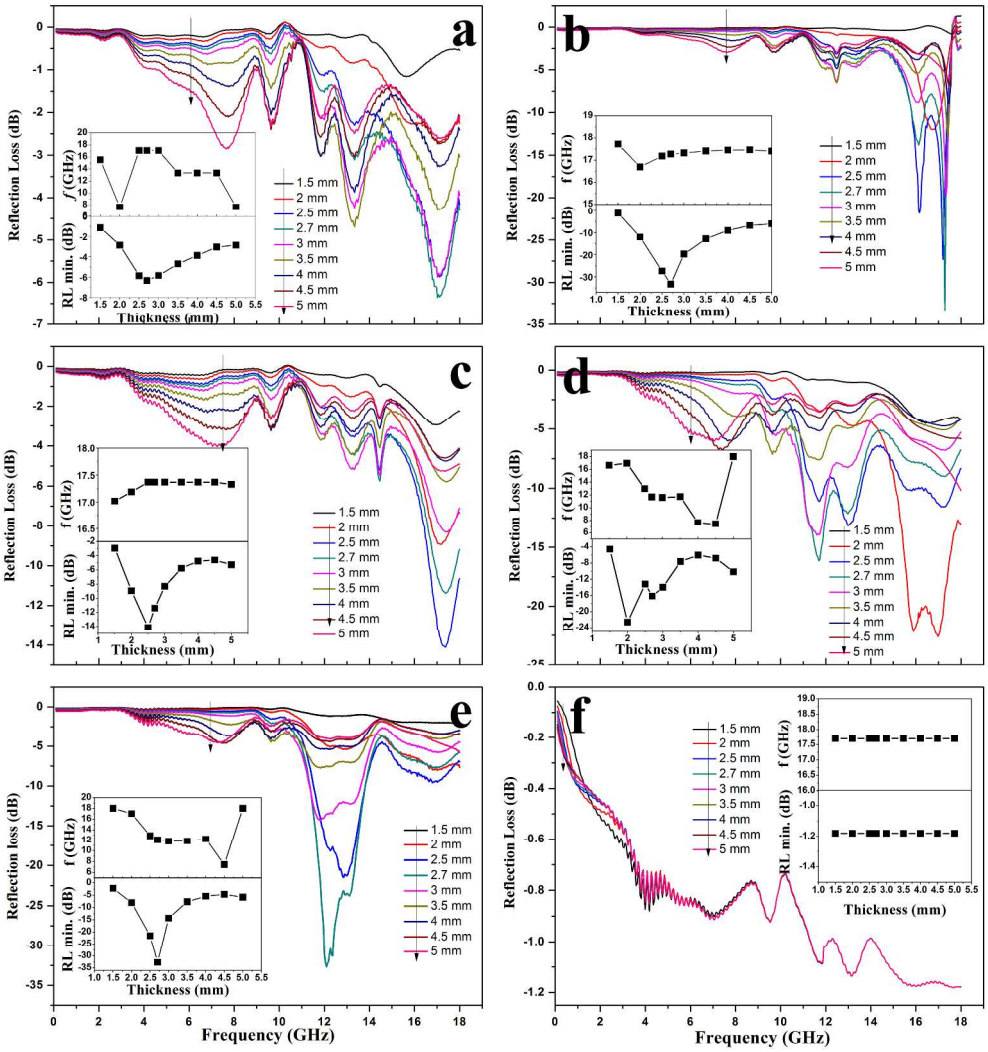

Fig. 6 Calculated RL curves of composites with different content of fillers (a, 3 wt.% ; b, 5 wt.%; c, 8wt.%; d, 10wt.%; e, 12wt.% and f, 15wt.%, respectively) and varied thickness according to a transmission line theory.
186x196mm (600 x 600 DPI)

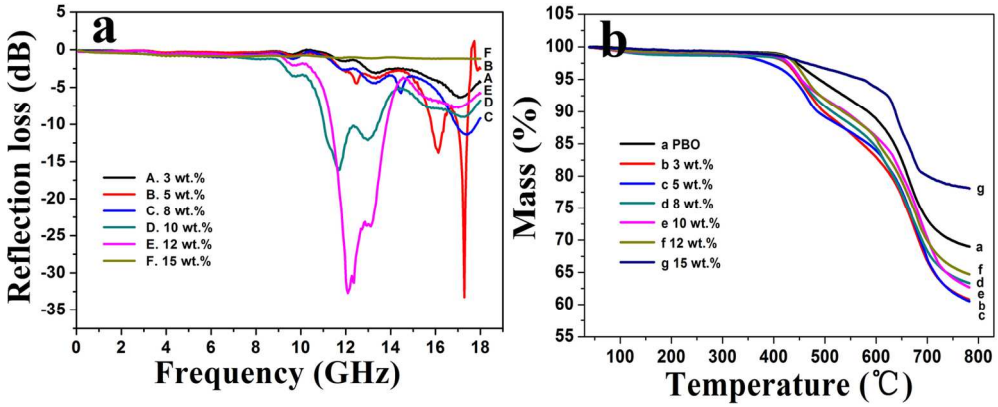

Fig. 7 (a) Microwave reflection loss of all the samples with the thickness of 2.7 mm. (b) TGA curves of the samples in nitrogen.
72x29mm (600 x 600 DPI)